The Pennsylvania State University

The Graduate School

DETERMINING THE EFFECT OF SILVER CONCENTRATION ON THE FORMATION OF SHAPE CONTROLLED SILVER NANOPARTICLES

A Thesis in

Chemistry

by

Susanna G. Ogozaly

Submitted in Partial Fulfilment
of the Requirement
for the Degree

Master of Science

August 2021

The thesis of Susanna G. Ogozaly was reviewed and approved by the following:

Robert M. Rioux
Friedrich G. Helfferich Professor of Chemical Engineering
Professor of Chemistry
Thesis Advisor

Raymond E. Schaak
DuPont Professor of Materials Chemistry
Professor of Chemical Engineering

Benjamin J. Lear
Associate Professor of Chemistry
Associate Department Head for Facilities

Phil Bevilacqua
Distinguished Professor of Chemistry
Distinguished Professor of Biochemistry and Molecular Biology
Department Head, Chemistry

Abstract

Synthesis of nanostructures have become incredibly valuable to fields such as catalysis, optics, and electronics. Solvent-based methods to produce shape-controlled nanoparticles (NP) are of particular interest due to the tunability of properties of the NP in addition to a potentially scalable, benchtop reaction. The goals of many of the studies investigating NP synthesis are to understand the mechanism of the NP formation, as well as, creating more environmentally friendly NP with properties more effective for their selected applications. Unfortunately, the mechanisms of many NP syntheses remain elusive. Countless methods have been established to create shape-controlled NP; however, the exact role of some components, like ligands or foreign metal additives, are unknown throughout the formation process. Ag nanocubes (NC) and octahedron are shape-controlled metal NP that have recently been investigated to understand the mechanism of these syntheses.

Throughout the work presented within this study, synthesis of Ag NC was investigated at several concentrations of Ag^+ which alters the polyvinylpyrrolidone to Ag ratio. The mechanism of synthesis was found to be the Finke-Watzky, two-step mechanism at multiple Ag^+ starting concentrations. It was also discovered that as starting concentrations of Ag^+ are increased, the diameter of the Ag NC increases as well. We hypothesize this is due to a constant number of Ag seeds being formed during the NC synthesis, resulting in roughly the same number of Ag NC in each synthesis of varying sizes depending on the free Ag^+. In addition to investigating Ag NC formation, the synthesis of Ag octahedron was investigated. The synthesis was found not to be reproducible under previously functional reaction conditions. The synthesis was probed to determine synthesis conditions that consistently produced octahedron. A higher formation temperature along with freshly synthesized Ag NC seeds were needed to result in Ag octahedron formation. The mechanism of synthesis is still under investigation. This work can collectively be used to advance understanding of what the role of each component is throughout Ag NP synthesis. As mechanisms are further understood, NP synthesis can be tuned more efficiently within the nanochemistry field.

Table of Contents

List of Figures

List of Tables

List of Abbreviations

NP (nanoparticle)

SA (surface area)

SDA (structure directing agent)

PVP (polyvinylpyrrolidone)

Ag NP (silver nanoparticle)

NC (nanocube)

EG (ethylene glycol)

GRR (galvanic replacement reaction)

SRP (standard reduction potential)

UPD (underpotential deposition)

HOMO (Highest occupied molecular orbital)

LUMO (lowest unoccupied molecular orbital)

SERS (Surface enhanced Raman scattering)

LSPR (Localized surface plasmon resonance)

OHN (octahedron)

PDO (1,5-pentanediol)

ICP-OES (Inductively coupled plasma optical emission spectroscopy)

SEM (scanning electron microscope)

SAXS (small angle X-ray scattering)

Acknowledgements

The work the material presented here was supported under the National Science Foundation (NSF) through grant number 500000001193. Disclaimer: All opinions, findings, recommendations, or conclusions displayed or expressed within this publication reflect the views of the author, and not necessarily the views of the NSF.

Scanning electron microscopy (SEM) images were obtained through the Microscopy Facility of the Penn State Huck Life Sciences. Small angle X-ray scattering (SAXS) data was obtained through the Materials Characterization Lab at the Penn State Materials Research Institute.

I would thank my advisor, Dr. Robert Rioux for his support and guidance during my time at Penn State. His knowledge and passion for catalysis allowed me to find a niche of nanoparticle synthesis and catalysis that I have greatly enjoyed working on and learning about. In addition, I want to thank Dr. Benjamin Lear and Dr. Raymond Schaak for agreeing to be a part of my committee and for all of their help, suggestions, and compassion.

I would also like to thank my group for similar reasons to my advisor. It has been wonderful to work and develop friendships with everyone. I would like to specially recognize Dr. Suprita Jharimune and Ms. Yanyu Mu. It was a privilege to have you all to become my friends, mentors, and coworkers.

I want to sincerely thank Dr. Kyle Schmid and Dr. Sheryl Dykstra for being phenomenal faculty that I had the pleasure of teaching under. Underneath the guidance I received while teaching organic chemistry, I was able to improve as an educator.

The final and most important acknowledgment is to thank my family and friends. I will be eternally grateful for the love and support of Jordan Hoinsky and my parents, John and Susan Ogozaly. I would not be where or who I am without you all. I also want to acknowledge Shannon McGee, Amanda Childs, Constance Selinsky, and Rebecca Balaj for their support and friendship throughout my time at Penn State University.

CHAPTER 1: INTRODUCTION

Background and History of Nanomaterials

Nanomaterials have been around for thousands of years, with some variations of nanoparticle (NP) synthesis beginning as early as the 14th century. Some more modern syntheses began in the late 19th and early 20th centuries with gold NP and SiO_2.[1] However, nanoscience as we know it began in the 1970-1980's with photochemistry and semiconductor chemists investigating colloidal CdS and TiO_2 to harvest solar energy.[2-4] Surface science as a whole was motivated by the energy crisis which called for new catalysts for oil and chemical processes.[5] In the 1990's this progressed to studying quantum dots of various metals created in colloidal syntheses.[2,6] Since then, the field of nanomaterials has expanded in several different directions for applications such as optics, electronics, catalysis, petroleum refining, and filler/stabilization for building products.[1,7-10] A major motivation for this work is to create more environmentally-friendly and efficient catalysts for these applications.

One reason NP are appealing for research in areas such as electronics and catalysis is that by changing the size of a material, the properties of the material can be altered drastically. Bulk materials compared to their nanomaterial counterparts can have differences in appearance, magnetism, melting point, and most importantly, properties which effect the catalytic ability of the metal.[11] One of the main factors that effects a metal's catalytic properties is surface area (SA), which is inversely proportional to the size of the NP. This can influence the metal's reactivity as a catalyst. For smaller NP, there are more surface atoms, which have a lower coordination number than the bulk atoms.[10,11] As the number of intramolecular interactions decreases, the reactivity of the atoms of the NP increases, which can lead to corner and edge atoms of NP being more reactive. However, catalysis or reactions often occur at atoms that are not on the edge or corner of a NP.

In addition to increased SA, electronic properties of the metals are altered due to changes in size. This is evident through properties such as ionization energy. Pt ionization energies were investigated by Taylor *et al.*[12] Ionization potential for Pt metal was approximately 5 eV, while the ionization potential for Pt single atoms and dimers

was higher, > 8 eV, suggesting the bulk Pt would ionize more easily.[10,12,13] The ability to undergo redox reactions is one of the most essential parts of catalysis, since it is an important aspect of most catalytic mechanisms. Therefore, affecting ionization energy will either increase or decrease catalytic efficiency, depending on desired properties of the catalyst. One reason the electronic properties of metals are transformed is due to metals experiencing the quantum size effect, which occurs because the electrons become more confined and the electron shells form more complex electron shells.[10,11,14] This then alters and widens the highest occupied molecular orbital – lowest unoccupied molecular orbital (HOMO-LUMO) gap due to increased energy levels.[10,11,14] The effects of altering a HOMO-LUMO gap are most evident for CdS and CdSe quantum dots, which change color due to changes in their band gap, and metals used in semiconductors, where the band gap is one of its defining features.[11,15] Alterations to HOMO-LUMO gap are also useful for stabilization which is evident from research by Bigioni and coworkers[16] that demonstrated that ultrastable Ag clusters could be synthesized partially due to a large energy gap.

In addition to size, shape further affects properties of the metals, such as polarization charge distribution, which controls the intensity and frequency of plasmon resonance.[17-21] These properties influence their applications to surface enhanced Raman scattering (SERS) and the localized surface plasmon resonance (LSPR), which are important in electronic, biological, and optical fields.[17-21] Other applications, like catalysis are also manipulated through alterations of shape/atomic configuration.[2,10,22,23] Research shows that different facets of the same NP can have different properties, potentially due to different binding energies of various molecules to the facets. Below, **Figure 1.1** demonstrates the different facets seen for some shapes of metal NP. It was discovered by Stamenkovic *et al.*[24] that the (111) facet of Pt_3Ni was more active than the Pt_3Ni (110) surface, which was in turn more active than the Pt_3Ni (100) surface for oxygen reduction, due to preferential OH binding. A similar case was investigated by Christopher and Linic,[25] where silver nanowires with (100) surfaces are more selective catalysts for formation of ethylene oxide from ethylene epoxidation than general silver spherical NP with (111) facets likely due to more favorable formation of a surface oxametallacycle intermediate on (100) than (111).[25] In general, several studies

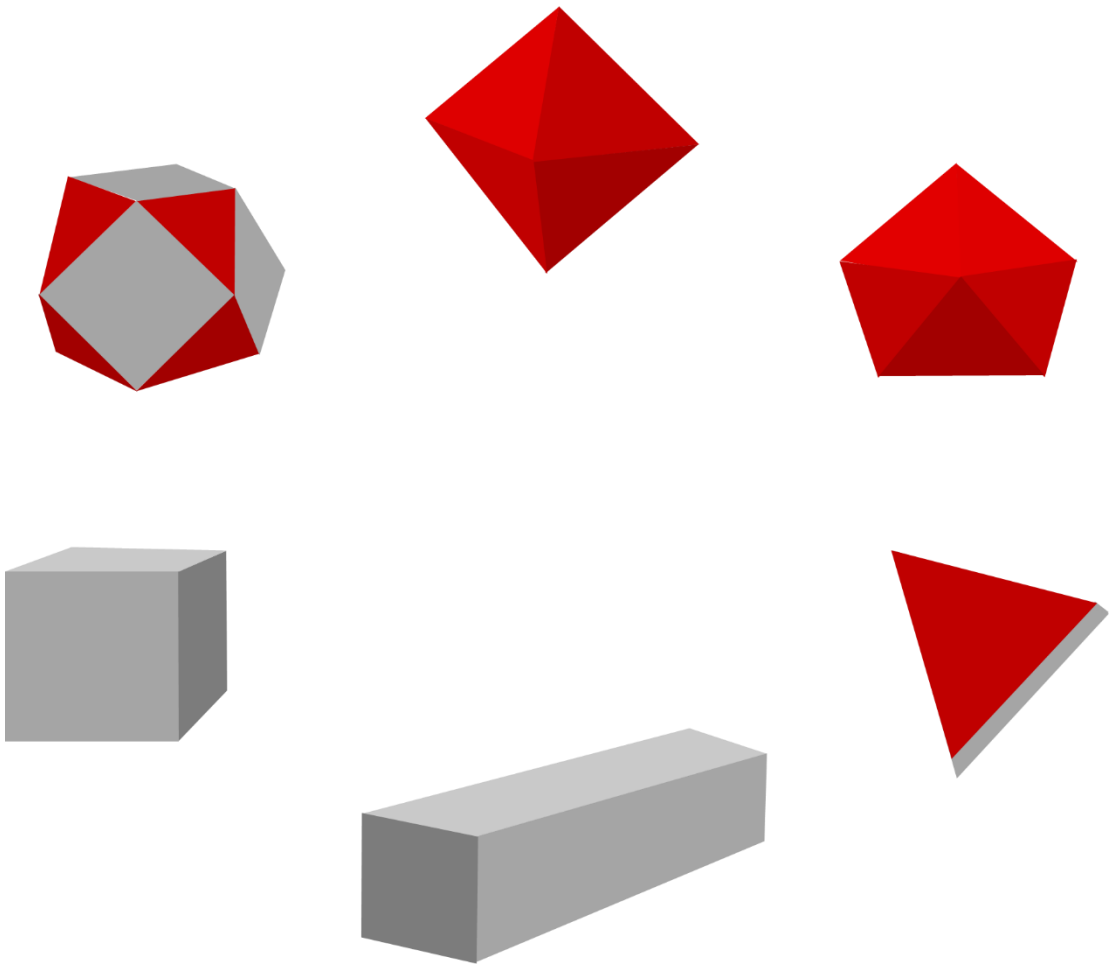

Figure 1.1: Several examples of some metal nanostructures able to be synthesized. The red corresponds to (111) facets, while the grey represents (100) facets. *Figure illustrated by Susanna Ogozaly.*

have concluded the facets exposed and NP shape during catalysis greatly affect the reaction selectivity and catalyst activity that can be completed with the NP.[22-26]

Synthesis Methods of Nanoparticles

In order to produce these shaped nanoparticles, solvent-based syntheses typically utilize a polyol solvent, and colloidal methods with capping ligands to stabilize the surfaces of the transition metal NP and prevent aggregation of the NP.[27-31] It is believed the ligands stabilize the surfaces of the NP due to reduction of surface charge which reduces NP surface energy.[32] Solvent-based synthesis of NP is advantageous over synthesis of other types of materials, like films and bulk, because NP formation allows for simpler tuning of properties for the NP through alterations of the synthesis conditions. In addition to their tunability, colloidal NP methods tend to be attractive due to simple, benchtop syntheses with a potential to be scaled for industrial application.[32]

The shape of the NP can be altered easily by altering synthesis conditions. The capping ligands used are thought to potentially act as structure-directing agents (SDA) in addition to stabilizing the surface of the NP.[23,26,33,34] Ligands have been found to bind preferentially to one facet of a NP over another, which may account for the ability to act as an SDA.[26] There are several types of capping agents commonly used in NP synthesis including polymers, like polyvinylpyrrolidone (PVP), halogens, and citrate.[23,26,33,35,36] PVP is widely used to create shapes such as cubes, wires, octahedra, and prisms for several metals including Ag, Au, Cu, Pd, Pt, and Ru.[23,35-41] In addition to the ligands, there are often other additives, like HCl, metal ions, halogens, etc., which can play a role in the NP syntheses as well.[17,26,42,43] Without these additives, the desired shapes for the NP are unlikely to form; however, it is not always well understood as to why a certain chape forms.[42,44] In the work of Kim *et al.*,[44] it was determined through experimentation combined with density functional theory (DFT) calculations that there was a collaborative effect between the capping ligand, hexadecylamine, and the additive, Cl^- (introduced by $CuCl_2$ and NaCl), to create copper nanowires.[44]

Silver Nanoparticles

For this project, silver nanoparticles (Ag NP) are of particular interest. Various shapes of Ag NP have been produced including spheres, cubes, octahedra, nanowires, nanobars, nanorods and bipyramids to obtain Ag NP with desired properties.[19,22,35,45-47] Xia and coworkers[47] have established a method for the synthesis of Ag nanocube (NC) using $AgNO_3$, PVP, and HCl in ethylene glycol (EG). Additional studies have discovered the Ag NCs produced via this method are greatly influenced by the ratio of Ag to PVP (monomer) concentration, the concentration of $AgNO_3$, temperature, the concentration of Cl^-, and the end groups of the PVP.[35,36,48] It has also been hypothesized PVP is a SDA that stabilizes the NC, while EG is oxidized to glycolaldehyde, which helps to reduce the Ag^+ to Ag^0.[34,49-51] Despite all of these investigations, the full mechanism of Ag NC synthesis is still not fully understood. Several hypotheses have been proposed regarding NP formation, but one aspect of the mechanism heavily debated is whether the binding of the PVP, which acts as an SDA, leads to thermodynamically controlled or kinetically controlled growth of Ag NC. Previously, the main hypothesis was the NC formation was thermodynamically controlled because of preferential binding of the PVP on the (100) facets over the (111) facets due to lower interfacial free energy.[31,35,52,53] Recently, Xin and Fichthorn[28] completed molecular dynamic (MD) simulations demonstrating PVP forms a thicker layer on the (100) facet of Ag, rather than the (111). The simulations also suggested the mechanism was kinetically controlled because the binding selectivity difference from (100) to (111) was not significant enough to suggest thermodynamic control.[28] Recent experimental work from our group, agrees with this hypothesis that the mechanism is kinetically controlled rather than thermodynamically controlled. Measurements of adsorption isotherms of PVP with varying molecular weight on Ag NP were conducted which resulted in an adsorption constant of 2.8 M^{-1} for PVP on (111) and 5 M^{-1} for PVP on (100), demonstrating PVP only has a slight (factor of less than 2) preference for binding to Ag (100) facets. When this data was applied to a thermodynamic Wulff construction, it proved that conditions for thermodynamic control had not been met because the minimal difference in binding energy does not account for exclusively (100)-bound particles.[35]

Ag NC can be further reacted to create hollow, precious metal or bimetallic structures through galvanic replacement reactions (GRR).[40,50,54,55] The GRR reactions can occur with any metal that has a higher standard reduction potential (SRP) than the metal composing the NP. For example, Ag could replace NP composed of Zn because the SRP of Ag is 0.7996 V, while the SRP of Zn is -0.7628 V.[56] When the SRP is lower than Ag, the metal will deposit, traditionally as a monolayer, on a Ag NP via underpotential deposition (UPD).[54,57] This occurs because the metals with the higher SRP are reduced to their elemental form, causing them to deposit, while the lower SRP metals are oxidized, similar to reactions that occur at an anode and cathode.[54,55] Zhang *et al.*[55] studied Ag GRR with Pt, which started with Ag NC templates. After introduction of K_2PtCl_4, the Pt^{2+} source, the resulting NP were bimetallic Pt/Ag in the shapes of a hollow nanobox, heterodimer, multimer, or a popcorn-shaped NP depending on reagent concentrations and their order of addition.[55]

In addition to being intermediates for GRR, Ag NC can be used as seeds to create other shapes of Ag NP, such as Ag octahedron (OHN).[40,50] There are several different established synthesis methods of Ag OHN, one method used by Yang and coworkers[18] began with 1,5-pentanediol (PDO) as the polyol solvent and reducing agent, PVP as the capping ligand, and $CuCl_2$ as a metal precursor additive. It was shown that depending on when the synthesis was quenched, the shape of Ag NP received could be cube, truncated cube, cuboctahedron, truncated octahedron, or OHN. These different shapes of NP are shown in **Figure 1.2**. This suggests the Ag nanocrystal growth is kinetically controlled due to Ag preferentially depositing on the (100) facets, while preserving the (111) facets, turning the NC bound by (100) facets into a (111)-bound OHN. The exact role of Cu^{2+} is unclear, but the introduction of a foreign metal to shaped metal NP synthesis has been studied several times, with some metals previously used include Ni, Fe, Cu, and Ag.[18,57-59]. Previously, Ag^{+} has been introduced into the seed-mediated growth of a few shapes of Au NP. The UPD that occurs between the Ag and Au stabilizes the NP facets and helps to control the NP shape.[57] Similarly, Ni^{2+} was used with Pt NP to form multicubes, a branched Pt structure primarily (100)-bound with high-index facets at the junction of adjacent cubic components. The Ni^{2+} helped to selectively evolve (100) facets on the multicubes from (311) high-index facets.[58]

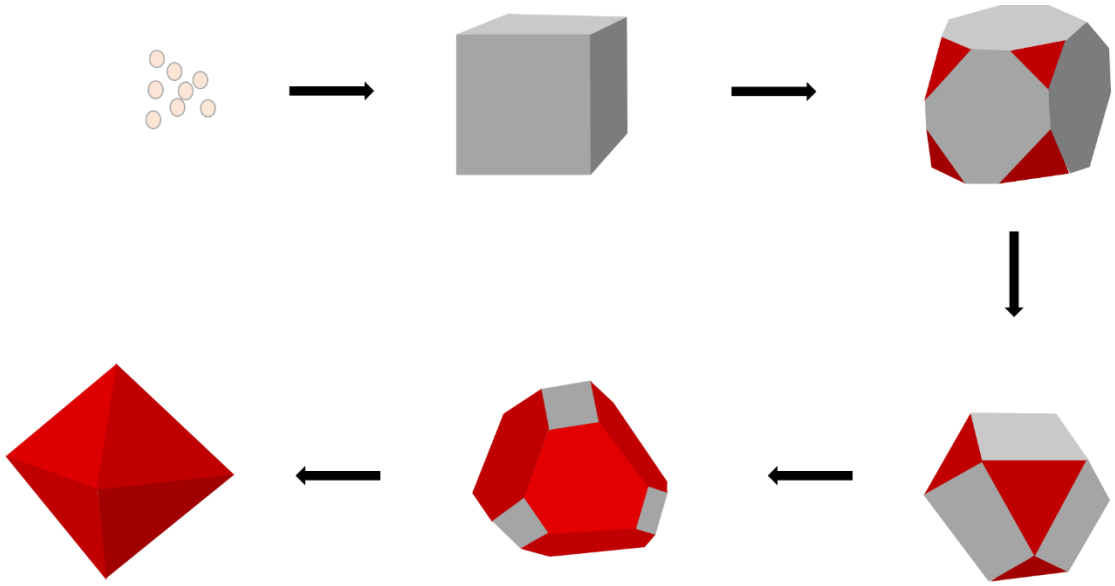

Figure 1.2: A diagram of the various shapes of Ag NP that are observed as Ag^+ deposits on the (100) facets of seed Ag NC to create (111)-bound Ag OHN. The red corresponds to (111) facets, while the grey represents (100) facets. *Figure illustrated by Susanna Ogozaly.*

Chapter 2. PROBING THE INFLUENCE OF SILVER CONCENTRATION (PVP:AG RATIO) ON THE RATE AND SIZE OF SILVER NANOCUBE SYNTHESIS

Background

Xia and coworkers[47] have done a great deal of work establishing the generally accepted method to synthesize Ag NCs. Some more recent work has focused on trying to understand the mechanism of the synthesis and what the role of each material is to creating NC. Previously, it has been ascertained that the structure of the Ag NC is influenced by both Cl^- (from HCl) and PVP.[35,42] It is also known the concentration of $AgNO_3$ and the ratio of $AgNO_3$ to PVP can affect the synthesis of the NCs.[48] It was believed that the EG is the main reducing agent for Ag^+ after it is converted to glycolaldehyde, and PVP is a stabilizing agent in addition to being a SDA because if its favored binding to specific facets.[49,51,60]

Recently, our group has focused on the role of the ligand, PVP, in the synthesis. Studies suggested that PVP may play a role in Ag reduction because at increased PVP to Ag ratios nanostructures other than NC were formed.[61,62] To examine the role of the ligand, the PVP end groups, PVP concentration (C_m), and PVP molecular weight (M_w) were varied. From variations of C_m and M_w at constant temperature and concentrations of Cl^- and Ag, an experimental phase diagram was created showing what Ag nanostructures are created under various PVP conititons.[36] This phase diagram demonstrates that at constant M_w, NC will form above a minimum C_m, and below a critical concentration. Above the critical concentration nanowires form. Another outcome of this work[36] was that reduction of Ag^+ was found to be proportional to the number of PVP end groups present and the chemical nature of the end groups present affected the NP produced. PVP terminated with an aldehyde group, a hydroxyl group, and an alkyl group were investigated resulting in monodisperse NC, a mixture of rods and NC, and irregular NP with AgCl cubes, respectively.

During the formation of the NC, AgCl is formed first, which dissolves to form the NC. This is shown in **Reactions 1** and **2**.[36]

$$AgCl\,(s) \rightleftharpoons Ag^+ + Cl^- \qquad (1)$$

$$nAg^{+} \longrightarrow Ag_n(s) \qquad (2)$$

The Ag^+ from **Reaction (1)** is reduced in **Reaction (2)**, driving **Reaction (1)** to the right. It is believed the aldehyde group on PVP has this reduction occur at a rate that allows Cl^- incorporation, but the hydroxyl group causes this same rate to be much faster, creating the kinetically favored Ag nanowires when the Cl^- does not have time to adsorb to the Ag. Because the inert PVP leaves AgCl unreacted, it was concluded **Reaction (2)** was slower and was not shifting **Reaction (1)** to the right to create more Ag^+. All of this data collectively lead to the conclusion that PVP end groups are the primary reducing agent in **Reaction (2)**. After this determination, the mechanism of reduction was hypothesized to follow the Finke-Watzky model which is a two-step process with a slow initial reduction rate, followed by an increased speed of reduction, referred to as autocatalysis.[36,63] This was supported by measuring the concentration of unreacted Ag^+ in solution as a function of time from 5 min to 33 h with a Ag ion selective electrode (ISE).

In the following work, a Ag ISE will be used to determine the concentration of Ag^+ as a function of time at several different concentrations of Ag^+ and Cl^-(constant Ag^+:Cl^- ratio) to determine how altering the PVP:Ag ratio affects the autocatalysis of NC formation. The motivation for this is the previous work[36] and other studies finding the ratio of PVP monomer to Ag can alter the NP formed during synthesis.[48] The temperature and concentration and molecular weight of PVP were held constant, while the Cl^- concentration was adjusted with the Ag^+ concentration, to maintain the Cl^-/Ag^+ from the standard synthesis. The PVP concentration (147 mM) and molecular weight (55,000 $g{\cdot}mol^{-1}$) and temperature (140°C) were selected because it has been found that the NC consistently and reproducibly form, in addition to being consistent with our previous work.[36] Cl^- concentration was adjusted to not affect **Reaction (1)** and formation of AgCl at the beginning of the synthesis. The results of this work will show increased concentration of Ag resulting in an increase in the rate of autocatalysis. The size of the NC was influenced by the concentration of Ag. Overall, the mechanism of Ag NC synthesis is not well understood, but recent research completed within this study

can potentially help the field better understand how each component of the synthesis plays a role in creating the NC.

Experimental

Chemicals:

Silver nitrate (99.9999%), polyvinylpyrrolidone (molecular weight ≈55,000 $g \cdot mol^{-1}$), and hydrochloric acid were obtained from Sigma Aldrich. Ethylene glycol (batch # 0000215539; 0000262046) was purchased from J. T. Baker. The glass vials used for the reactions were obtained from WVR (catalog number 89093-836) pre-cleaned. All chemicals were used as obtained.

Synthesis of Ag nanocubes by the polyol method:

A modified version of the synthesis reported by Xia was used.[47] For each standard synthesis, 2.5 mL ethylene glycol (EG) was pipetted into a 40 mL pre-washed glass vial with the cap not fully tightened. The EG in the vials was heated for 1 h in a silicone oil bath at 140°C with a Teflon-coated disposable stir bar spinning at a rate of 360 rpm. After heating for 1 h, 0.5 mL of a 3 mM hydrochloric acid in EG mixture was added. After an additional 10 min, 1.5 mL of two solutions, a 94 mM silver nitrate in EG and a 147 mM PVP (concentration based on monomer molecular weight) in EG, were injected concurrently via a syringe pump (Harvard Apparatus) from separate syringes at a volumetric flow rate of 45 $mL \cdot h^{-1}$. For 20 h, the vial caps were kept loosely affixed, then the caps were fully tightened. Importantly, it should be noted that NO gas is released during this synthesis, which potentially converts to NO_2 gas on exposure to air. Therefore, the reaction must be performed in a working, well-ventilated fume hood while wearing protective clothing. The vials were removed from the heated oil bath at 28 h. Hydrochloric acid was adjusted based on the silver concentration in a $1:31.\overline{3}$ molar ratio for reactions at a different silver concentration.

Characterization of Ag nanocubes via SEM:

Scanning electron microscope (SEM) images were obtained with a Zeiss Sigma Variable Pressure (VP) field emission SEM at a voltage of 3 kV with In-lens and SE2

detectors. Prior to imaging with the SEM, Ag NC were washed 3-5 times with 200 proof ethanol to remove EG and PVP. To image the NC, a slight amount (5-10 µL) of the NC suspended in ethanol was drop cast on silicon wafer pieces.

Quantification of autocatalytic kinetics by ion selective electrode measurements:

Ion selective electrode (ISE) measurements were performed with a Ag^{+}/S^{2-} combination ISE from Hanna Instruments (HI4115) filled with 1 M potassium nitrate (Hanna Instruments). The ISE probe was used with an Orion Star A214 pH/ISE meter (ThermoFisher Scientific). To prepare samples for ISE measurement, the NC in EG were cooled to approximately 25°C, before the samples were centrifuged for 30 min at 8500 rpm. From this, 2 mL of the solvent without suspended Ag NC was diluted to 10 mL with water, then 0.2 mL of ion strength adjuster (ISA, Hanna Instruments) was also added. The ISE was calibrated before to each use using several dilutions of a 0.1 M silver calibration solution (Hanna Instruments). All standards and samples were continuously stirred during the measurements.

Results and Discussion

Standard Ag NC were synthesized by heating EG to 140°C, then adding 0.5 mL of 3 mM HCl in EG. After 10 min, 1.5 mL of 147 mM PVP (55,000 $g \cdot mol^{-1}$) in EG was added at the same time as 1.5 mL of 94 mM $AgNO_3$ in EG. This was allowed to react and stir for 20 h with the caps loosely affixed to enable diffusion of air into the vials. After an additional 8 h, the vials were removed from the oil bath and allowed to cool to room temperature. When NC were synthesized at different concentrations of Ag, the HCl concentration was adjusted to ensure the Cl^{-}/Ag^{+} ratio remained in a $1:31.\overline{3}$ ratio. The reason behind this adjustment is that with more Ag present, you would need increased amounts of Cl^{-} to not affect **Reaction (1)**, to form AgCl, and to help direct the cube formation. **Table 2.1** reflects all of the conditions explored, the ratio of PVP to Ag, and whether NC were able to be formed.

From **Table 2.1**, the higher and lower limits of the PVP:Ag ratio (based on PVP monomer concentration) which produce Ag NC can be ascertained. The lowest PVP:Ag ratio is 1:1.02 because the highest Ag^{+} concentration to successfully produce

Table 2.1: Reaction concentrations used to create Ag nanoparticles at 140°C, with 147 mM PVP (based on monomer concentration) in a 6 mL reaction volume. All vial caps were tightened at 20 h after the addition of PVP and $AgNO_3$. The standard synthesis is designated by a box around the row. NC indicates nanocube formation; mix indicates a mix of cubes, rods, and irregular NP.

Ag^+ (mM)	HCl (mM)	PVP : Ag	NP Formed
50	1.6	1:0.34	Mix
55	1.76	1:0.37	NC
75	2.39	1:0.51	NC
94	3	1:0.64	NC
115	3.67	1:0.78	NC
150	4.7	1:1.02	NC
200	6.3	1:1.36	Mix

NC was 150 mM. Similarly, 55 mM Ag^+ was able to form NC, resulting in the highest PVP:Ag ratio of 1:0.37. In **Figure 2.1**, the Ag NP produced for each of the syntheses from **Table 2.1** are summarized. In both **Figure 2.1.A** and **Figure 2.1.G,** there are a mixture of shapes, but the primary NP observed is Ag nanorods. However, at 50 mM Ag (**Figure 2.1.A**) there are numerous cubes that are rounded, with non-sharp edges, while the 200 mM Ag sample (**Figure 2.1.G**) has few cube NP, but the cubes produced have noticeably sharp edges. Because the main Ag NP formed was not NC, these were considered to be failed experiments. For all other concentrations of Ag (**Figure 2.1.B-F**) cubes with sharp edges were the main observed Ag NP, with few rods and bipyramids observed throughout the SEM samples, proving they were successful NC syntheses.

The SEM images further provide information about the size of the Ag NC. From the SEM images, the average size was estimated for the NC at each Ag concentration. The average size of the cubes is below in **Table 2.2**. From this table, it is shown that as the concentration of Ag is increased, the average size of the NC increased. The increased size of the NC with increasing Ag^+ and Cl^- concentrations is likely due to a constant number of Ag seeds being formed during the synthesis of the NC. If the concentration of Ag^+ had control over the number of NC formed, there would not be a significant difference in NC sizes from one synthesis to another. Instead, there would only be more or less cubes formed due to the amount of Ag introduced to the system.

Sizes of the NC were found to be influenced by the PVP:Ag ratio as shown in **Table 2.2**. The data was examined to determine if there was a consistent correlation between the changes in PVP:Ag ratio and edge length of the Ag NC. The edge length of the Ag NC formed from a solution of 150 mM (126.7 nm) was 28% larger than the Ag NC formed in the standard synthesis (91.7 nm) where the ratio of PVP:Ag is 1.6 times smaller. For the 55 mM Ag NC synthesis, the PVP:Ag ratio was increased by a factor of ~2 from the 94 mM Ag synthesis, which resulted in a ~16% smaller size of Ag NC. **Figure 2.2** represents the Ag NC edge length vs Ag^+ concentration. It is evident that there is an exponential relationship between the measured size of the NC and the

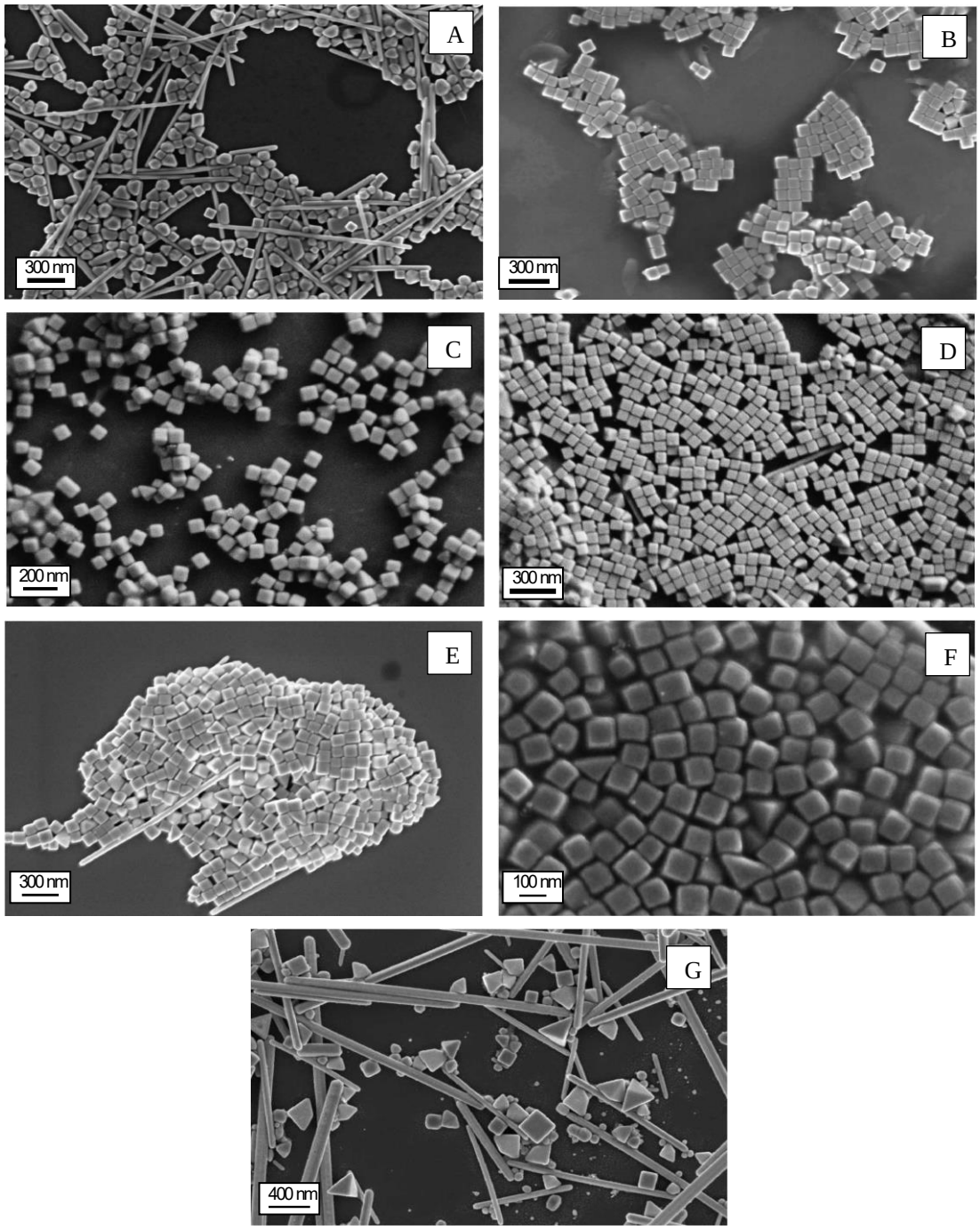

Figure 2.1: SEM images of the Ag nanoparticles formed under different Ag and HCl concentration, at 140°C, with 147 mM PVP in a 6 mL reaction volume. All vial caps were tightened at 20 h after the addition of PVP and $AgNO_3$. **(A)** 50 mM Ag, 1.6 mM HCl; **(B)** 55 mM Ag, 1.76 mM HCl; **(C)** 75 mM Ag, 2.39 mM HCl; **(D)** 94 mM Ag, 3 mM HCl; **(E)** 115 mM Ag, 3.67 mM HCl; **(F)** 150 mM Ag, 4.7 mM HCl; **(G)** 200 mM Ag, 6.3 mM HCl.

Table 2.2: Ag NC sizes obtained from synthesis at varied Ag^+ and Cl^- concentrations. All syntheses heated to 140°C, with 147 mM PVP in a 6 mL reaction volume. All vial caps were tightened at 20 h after the addition of PVP and $AgNO_3$. Size is believed to be the result of a constant number of Ag seeds formed with the amount of free Ag^+ being used to create roughly the same number of NC for each synthesis. The standard synthesis is designated by a box around the row.

Ag (mM)	Average Diameter of NC (nm)	Standard Deviation (nm)
55	77.4	±10.8
75	83.0	±6.5
94	91.7	±7.2
115	103.6	±8.3
150	126.7	±13.1

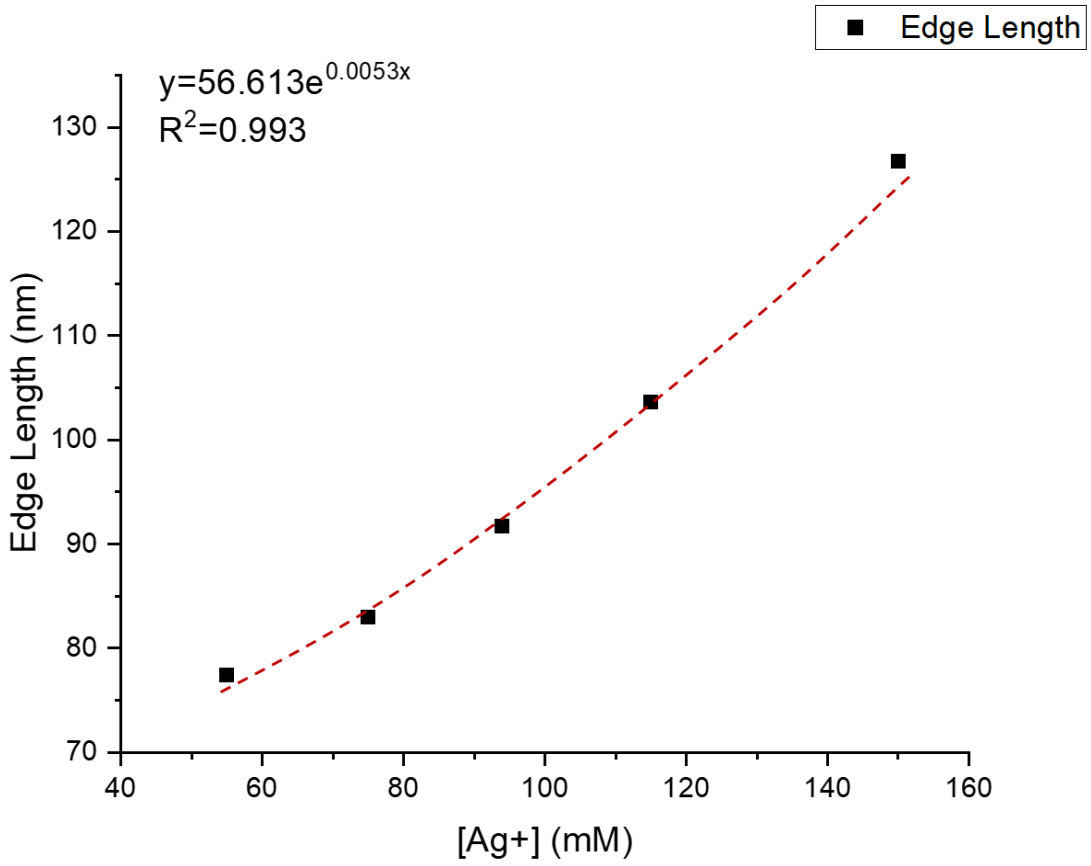

Figure 2.2: Measured edge length of synthesized Ag NC as a function of various concentrations of Ag^+. All synthesis occurred at 140°C with 147 mM PVP in a 6 mL reaction volume, and all vial caps were tightened at 20 h after the addition of PVP and $AgNO_3$.

concentration of Ag^+. Therefore, it is observable that at decreased PVP:Ag ratio but increased Ag^+ concentration the diameters of Ag NC will exponentially increase.

Despite the size differences between the NC, all syntheses underwent the same appearance and color changes. **Figure 2.3** shows the general color progression of a normal Ag NC synthesis as time progresses. The color changes observed are typical of all NC syntheses performed, regardless of the Ag^+ concentration being investigated. However, the time at which each color change occurred varied from one Ag concentration to another. All reactions remained clear and colorless (**Figure 2.3.1**) until 20 h when the caps were closed. After 20 h, the higher concentrations of Ag^+ progressed through the reaction and color changes more quickly than the lower Ag^+ concentrations. The slowing down of the reactions with lower Ag^+ is likely due to diluting the reaction mixture, which is known to decrease the probability of molecular interactions.

In order to understand how the autocatalysis of the NC formation was affected by altering the PVP:Ag ratio, the standard synthesis was repeated first to ensure all prior results were repeatable, and to observe average Ag concentrations as a function of time, rather than individual reactions. The Ag ISE results from measuring several time points during a 94 mM Ag^+ NC synthesis are demonstrated in **Figure 2.4.** The recent data is compared to some of the data from our group's most recent publication.[36] The main difference is the recent data, shown as black boxes, is an average of two or more reactions, with all of the points representing the autocatalysis steps representing at least four or more reactions. The point considered to be the start of autocatalysis is denoted with a '*' above the data on the graph. The published data, shown as red circles, represents only one reaction that is a relatively accurate reflection of a standard synthesis at that time point.

As evidenced by the error bars in **Figure 2.4**, there can be quite a bit of variation in the measured quantity of Ag^+, especially during the autocatalytic steps of the reaction. The reactions are complete at approximately 28 h from the start; however, it is common to have a reaction finish slightly faster or slower ($\pm$1 h) than 28 h. This slight variation s not significant at early time points during the initial reduction by the PVP because it is a slow step, allowing variation in concentrations to remain small. The

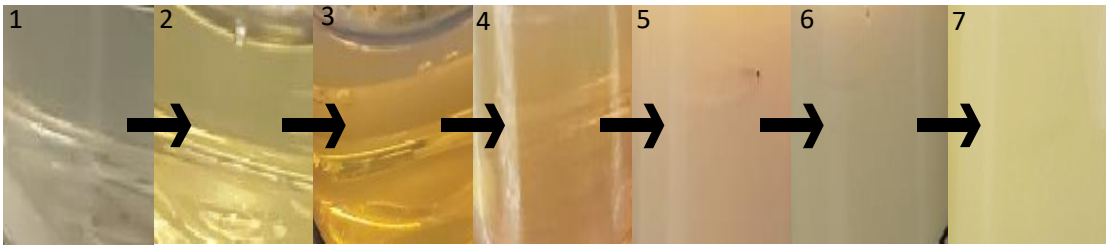

Figure 2.3: Color changes as the synthesis of Ag NC progresses from left to right. The synthesis begins as a clear, colorless solution **(1)** then progresses to a clear yellow sometime after the vial caps are tightened at 20 h **(2)** before becoming an increasingly more opaque yellow solution **(3-4).** As the NC begin to more quickly around the start of the autocatalysis, the solution becomes red-orange and remains opaque **(5**) then progresses to a green solution with a red tint **(6).** The final, finished NC synthesis appears as a fully opaque muddy, green-brown or green-tan **(7).** All syntheses are completed at 140°C with 147 mM PVP.

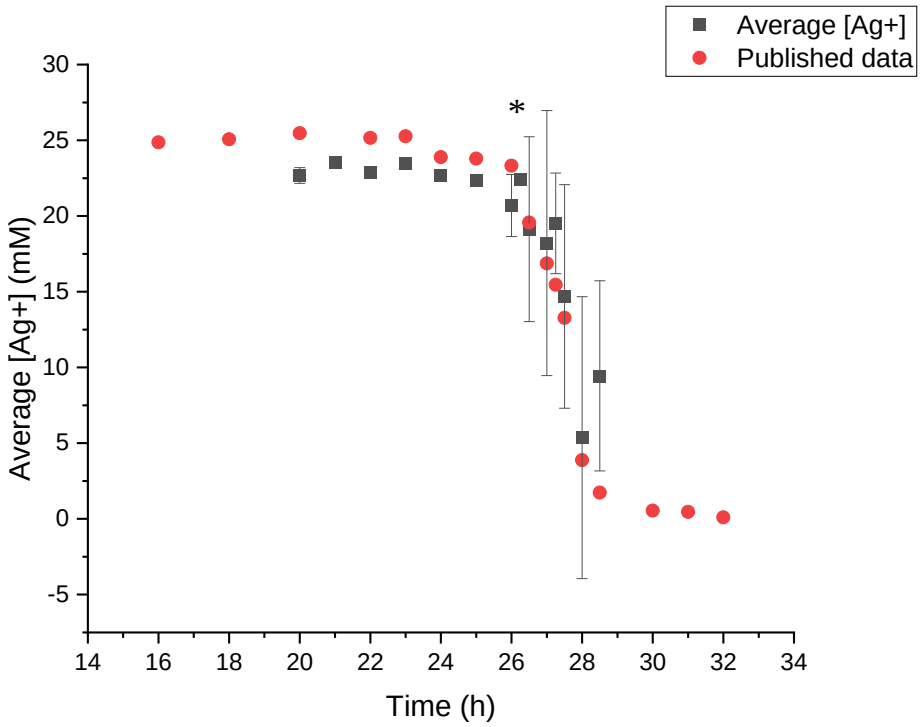

Figure 2.4: Concentration of Ag^+ measured via a Ag ion selective electrode as a function of time during Ag NC formation. Black squares represent recently measured reactions, with each point being two or more averaged reactions. Red circles represent individual reactions measured previously by our group.[35] All NC were synthesized at 140°C, with 147 mM PVP, 94 mM $AgNO_3$, and 3 mM HCl in a 6 mL reaction volume. All vial caps were tightened at 20 h after the addition of PVP and $AgNO_3$. * designates the beginning of the second step of the mechanism (autocatalysis).

averaged, new data (black squares) are similar and comparable to the previous, published data (red circles). Most time points are approximately the same concentration of Ag^+. Some of the minor differences between the two sets of data can be attributed to the variation in the individual reactions in addition to potential fluctuations in reaction temperature and air flow within the fume hoods where the reactions took place. All of the NC produced from the reactions shown in **Figure 2.4** were characterized via SEM. The images of the NC appeared similar to **Figure 2.1.D**.

After the standard synthesis was investigated, Ag^+ concentrations of 55 mM, 75 mM, and 150 mM were investigated to ascertain changes to the kinetics of the NC formation caused by alterations to the PVP:Ag ratio. The first concentration investigated was 150 mM Ag. In order to synthesize the Ag NC at this Ag concentration, 150 mM $AgNO_3$ in EG and 6.3 mM HCl in EG were substituted in place of the standard $AgNO_3$ and HCl concentrations. This resulted in Ag NCs with an average diameter of 126.7 nm that were fully synthesized after ~27 h. **Figure 2.5.C** shows the measured Ag^+ concentration as a function of time. Due to the slight variation in reactions, it was decided that the time points should be no closer than 0.25 h apart to ensure the time points were likely to be distinct. From a time of 0 h to ~24 h there was no significant change in the concentration of Ag^+. Because the 150 mM Ag synthesis was much faster than the standard synthesis, it was difficult to measure the individual Ag^+ concentration during the autocatalytic phase of the reaction. Only the beginning of the autocatalysis was able to be measured and all further time points showed to be near completion of the reaction. The beginning of the autocatalysis is designated with a '*' in the graph. It is likely the autocatalysis will not be able to measured *ex-situ* for this synthesis due to the increased speed of the NC formation.

In order to accurately measure the autocatalytic portion of the NC synthesis, the next system studied was chosen to be 75 mM Ag NC because it had a lower PVP:Ag ratio, which led to the hypothesis that NC formation would be slower than the standard synthesis. To create these Ag NC, 75 mM $AgNO_3$ and 2.39 mM HCl in EG were used in place of 94 mM and 3 mM solutions, respectively. The previously mentioned hypothesis was proven correct as Ag NC synthesis was finished after ~30 h resulting

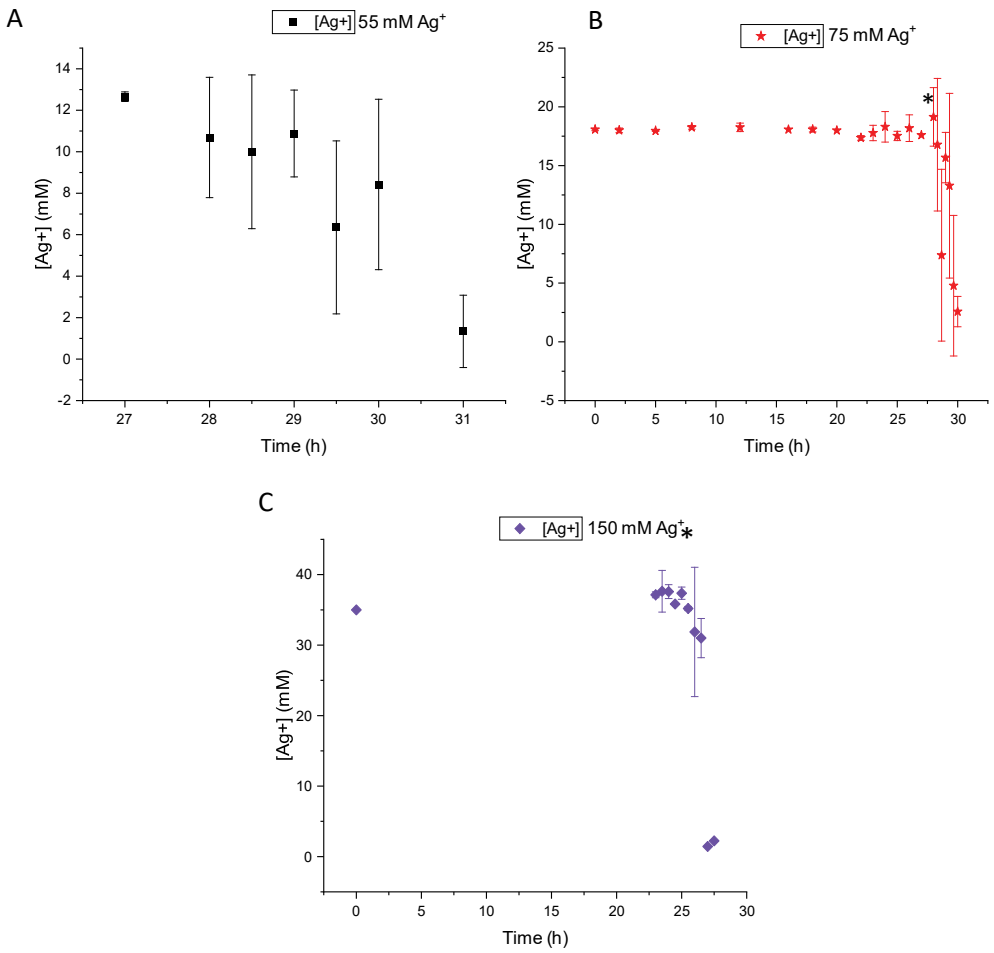

Figure 2.5: Ag concentration versus time for three different starting concentrations of Ag measured with Ag ISE. **(A)** 50 mM Ag starting concentration from 27 h to 31 h. **(B)** 75 mM Ag starting concentration from 0 h to 30 h. **(C)** 150 mM Ag starting concentration from 0 h to 28 h. All syntheses were heated to 140°C with 147 mM PVP, and caps were closed at 20 h. * designates the being of the second step of the mechanism (autocatalysis).

in cubes with a diameter of 83.0 nm. The Ag ISE results presented in **Figure 2.5.B** shows a constant Ag^+ concentration until ~26 h, followed by the autocatalysis occurring at approximately 28 h. Similar to the previous Ag concentrations, the variation from one reaction to another at the same time point lead to large standard deviations around the point of autocatalysis. However, **Figure 2.5.B** details the changing Ag^+ concentration well, and agrees with **Figure 2.4** that the Ag reduction likely follows the two-step, Finke-Watzky mechanism.

The final system investigated was 55 mM Ag^+, which was hypothesized to be slower than the 75 mM Ag synthesis, and result in smaller cubes. In order to produce the 55 mM Ag NC, 55 mM $AgNO_3$ in EG in combination with 1.76 mM HCl in EG were used in place of the standard concentrations of Ag^+ and Cl^-. This synthesis did indeed produce the smallest viable cubes, with an average diameter of 77.4 nm. Limited Ag ISE data for 55 mM Ag NC synthesis is shown in **Figure 2.5.A**. Due to several factors, a complete graph starting from 0 h demonstrating the concentration of Ag^+ as a function of time was not able to be constructed. It is hypothesized that the concentration of Ag^+ would remain constant until ~27.5 h, with the autocatalysis beginning at approximately 29.25 h. Based on full syntheses completed, it was observed by eye that the synthesis was complete at ~32 h.

In conclusion, as the PVP:Ag ratio changes the NC size and speed of the NC formation are also altered. The increased sizes of NC at lower PVP:Ag ratios is believed to be the result of a constant number of Ag seeds being formed during the Ag NC synthesis. Theoretically, for each reaction the same number of Ag seeds and NC are created, with size changing based on the available Ag^+. If the quantity of Ag seeds changed, the number of NC formed per synthesis would be the only difference between the various Ag^+ concentrations. Additionally, the speed of the NC formation was dependent on the PVP:Ag ratio, but based on the 75 mM, 94 mM, and 150 mM Ag ISE data that showed Ag^+ concentration against time, the NC formation follows the two-step Finke-Watzky mechanism at multiple PVP:Ag ratios.

CHAPTER 3. PROBING THE APPROPIATE AND REPRODUCIBLE EXPERIMENTAL CONDITIONS FOR THE FORMATION OF SILVER OCTAHEDRON

Background

There are several methods proven to form Ag OHN, with some employing Cu^{2+} as a common reaction additive.[40,50,64] Previously work within our group employed a modified version of the synthesis route outlined by Yang and coworkers.[64] In this synthesis, $AgNO_3$ is used as the metal precursor, PVP is used as the capping ligand and potentially reducing agent, $Cu(NO_3)_2$ or $CuCl_2$ is used as a Cu^{2+} source, and 1,5-pentanediol is the polyol solvent and another potential reducing agent. During this synthesis, depending on the time the synthesis is quenched, the shape of the Ag NP ranges from a cube to an OHN, with the different possible Ag NP shapes highlighted in **Figure 1.2**. Based on the various obtainable shapes, it was originally hypothesized the synthesis is kinetically controlled by selective deposition on the (100) facets, resulting in (111)-bound Ag NP. However, the role of the Cu^{2+} and the deposition of the Ag^{+} on the (100) surfaces are not known. With this information, our group focused on the role of Cu^{2+} and other foreign metals on the synthesis of Ag OHN from Ag NC to determine if the growth of the OHN is kinetically or thermodynamically controlled.

The metal ions studied by our group included Cu^{2+}, Co^{2+}, Ni^{2+}, Au^{3+}, and Pd^{2+}. These metals were chosen specifically due to Cu, Co, and Ni having lower SRP, while Au and Pd have higher SRP. Therefore, the lower SRP metals may utilize UPD, while the metals with high SRP involved GRR. All the metals were found to synthesize the Ag OHN, but the Pd and Au resulted in only an approximate 50% conversion to the OHN, due to GRR. The initial GRR creates holes in the seed Ag NC, which are repaired by the continuous addition of Ag^{+} and PVP. However, this leaves less free Ag^{+} and PVP to form the OHN. A synthesis without the presence of any metal ion produced only irregular shaped-Ag NP. Another important aspect of the synthesis investigated was whether Cl^{-} was necessary for shape control. The source of Cl^{-} was only from $CuCl_2$, so a control experiment was completed, resulting in Ag OHN formation with $Cu(NO_3)_2$, proving Cl^{-} has no influence over the Ag OHN synthesis, like it does for the

Ag NC synthesis. Because Cl^- was not necessary for synthesis, our group employed only nitrate salts (except for Au^{3+}, since Au nitrate is not commercially available) to avoid AgCl formation.

The outcome of the work completed experimentally by our group, in combination with density functional theory (DFT) calculations was the theory that based on thermodynamic considerations the foreign metals adsorb either through UPD or GRR on the (100) facets due to lower formation energies compared to the (111) facets. This deposited foreign metal is then oxidized as it reduces Ag^+ to Ag^0 on the (100) facets, in addition to a possible small amount of Ag^+ being reduced by the solvent or PVP on both the (100) and (111) facets. These processes can be observed in **Figure 3.1** as steps **1,2,** and **A**.

In the following work, it will be discussed that the Ag OHN synthesis method previously used by our group has proven not to be repeatable in another location by another researcher. To successfully recreate Ag OHN, the age of the Ag NC seeds, the moles of Cu^{2+} added into the system, the flasks, flow rate, and temperature were all manipulated. It was discovered that fresh Ag NC (<14 days old) need to be used in addition to a slightly increased temperature to what has previously been used by our group.[35] Both 500 $\mu L \cdot min^{-1}$ and 400 $\mu L \cdot min^{-1}$ volumetric flow rates of Ag^+ and PVP resulted in Ag OHN formation. It was also observed that a lower concentration of Cu^{2+} than the standard synthesis do not result in Ag OHN, despite previous work indicating otherwise. Once the reaction was found to produce Ag OHN, the kinetics were attempted to be investigated via Ag ISE by measuring the concentration of Ag^+ as a function of time, similar to the Ag NC. Unfortunately, the results thus far do not definitively point at a mechanism for the formation of the Ag OHN.

Experimental

Chemicals:

Silver nitrate (99.9999%), polyvinylpyrrolidone (molecular weight ≈55,000 $g \cdot mol^{-1}$), copper nitrate hydrate were obtained from Sigma Aldrich. 1,5-pentanediol (PDO) was obtained from Acros Organics. All chemicals were used as obtained. Ag

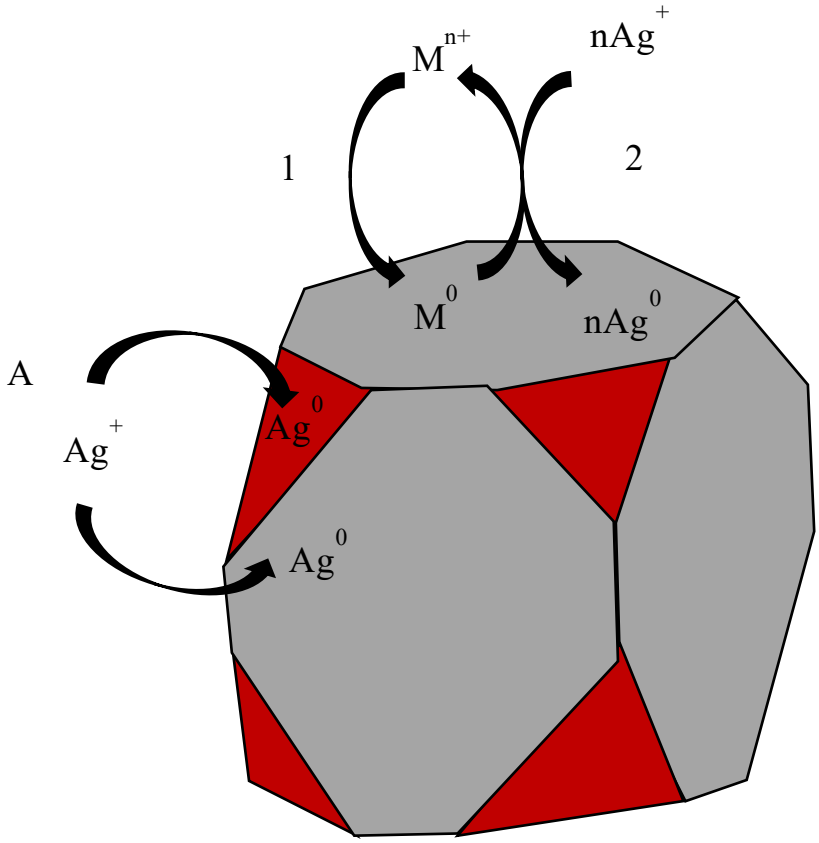

Figure 3.1: Proposed general model of Ag OHN formation assisted by foreign mental ions, denoted as M, the grey sides denote the Ag (100) facets, while the red sides denote the (111) facets. **(1)** The foreign metal adsorbing to the (100) surface (grey) of the Ag NC seed either through UPD or GRR depending on the metal's SRP. **(2)** The reduction of Ag^{+} to Ag^{0} onto the (100) facet (grey) aided by the foreign metal being oxidized from M^{0} back to M^{n+}. **(A)** Some Ag^{+} is reduced by the solvent or PVP to Ag^{0} on both (100) facets (grey) and (111) facets (red). *Figure illustrated by Susanna Ogozaly.*

seed NC were synthesized following the method provided in the Chapter 2: Experimental section" *Synthesis of Ag nanocubes by the polyol method"*.

Synthesis of Ag octahedron from Ag nanocube seeds

The Ag NC seeds were removed from the EG and excess PVP by cleaning with ethanol and centrifugation approximately five times. The clean NC were then redispersed in 6 mL ethanol before two thirds of the suspension was transferred to a 2-neck, 250 mL round bottom flask. The ethanol was removed via rotor evaporation, then the NC were resuspended in 6 mL of PDO. 1 mL of 180 mM PVP (concentration based on monomer molecular weight) in PDO and 50 µL of a 3.44 mM $Cu(NO_3)_2$ in PDO were then added. The flask was then heated from room temperature until approximately 195°C with a stir rate of 550 rpm. A programmed temperature control box was used to heat the oil bath. Once heated, 235 mM $AgNO_3$ and 180 mM PVP were added simultaneously via syringe pump (Harvard Apparatus) with a flow rate of 500 µL·min^{-1} from separate syringes. Aliquots were removed from the synthesis periodically to observe the NP formation. Ag OHN were typically obtained after 25-35 min.

Characterization of Ag nanocubes via SEM:

Scanning electron microscope (SEM) images were obtained with a Zeiss Sigma Variable Pressure (VP) field emission SEM at a voltage of 3 kV with In-lens and SE2 detectors. Prior to imaging with the SEM, Ag OHN were washed 3-5 times with 200 proof ethanol to remove PDO and PVP. To image the OHN, a small amount (5 µL) of the OHN suspended in ethanol was drop cast on silicon wafer pieces.

Quantification of kinetics by ion selective electrode measurements:

Ion selective electrode (ISE) measurements were performed with a silver/sulfide combination ISE from Hanna Instruments (HI4115) filled with 1 M potassium nitrate (Hanna Instruments). The ISE probe was used with an Orion Star A214 pH/ISE meter (ThermoFisher Scientific). To prepare samples for ISE measurement, the OHN in PDO were cooled to approximately 25°C, before the samples were centrifuged for 45 min at 8500 rpm. From this, 4 mL of just the solvent was diluted to 10 mL with water, then 0.2 mL of ion strength adjuster (ISA, Hanna Instruments)

was also added. The ISE was calibrated before to each use using several dilutions of a 0.1 M silver calibration solution (Hanna Instruments). All standards and samples were continuously stirred during the measurements.

Quantification of Copper by Inductively Coupled Plasma Optical Emission Spectroscopy:

Inductively coupled plasma optical emission spectroscopy (ICP-OES) was used to determine the true concentration of Cu^{2+} in a Cu nitrate hydrate stock solution in PDO, due to the hydrate being unspecified. To prepare samples, the stock solution was diluted in 2% HNO_3. The ICP-OES was calibrated prior to each use with several dilutions of a 100 $\mu g \cdot mL^{-1}$ Cu^{2+} standard (Inorganic Ventures).

Results and Discussion

Standard Ag OHN were synthesized by adding cleaned Ag NC into a 2-neck round bottom flask, evaporating off the ethanol, then resuspending the seeds in 6 mL of PDO. 1 mL 180 mM PVP (55,000 $g \cdot mol^{-1}$) and 50 µL 3.44 mM $Cu(NO_3)_2$ (0.172 µmoles Cu^{2+}) in PDO were added before the flask was heated from ~25°C to ~190°C. Once the temperature measured was above 190°C for the oil bath, 180 mM PVP and 235 mM $AgNO_3$ in PDO were added at a rate of 500 $\mu L \cdot min^{-1}$. By 20-35 min Ag OHN were visible by SEM if a synthesis was successful.

To begin the work with the kinetics of Ag OHN, the standard synthesis was attempted to be repeated; however, while attempting to produce the Ag OHN, the products of the syntheses were repeatedly irregularly shaped, almost rounded Ag NP with either few or no OHN. **Figure 3.2** shows examples of unsuccessful synthesis products. After multiple attempts to produce the Ag OHN without success, it was determined that the issue(s) were likely due to one or more problems with the synthesis conditions. The conditions altered in an attempt to successfully synthesize Ag OHN included the NC being changed to freshly synthesized (less than 14 days old), different amounts of moles of Cu^{2+} were utilized, new, unscratched round bottom flasks were employed, a slower flow rate, and temperature was adjusted. Fresh Ag NC were used in the synthesis due to the observation that Ag NC that were dispersed in ethanol for

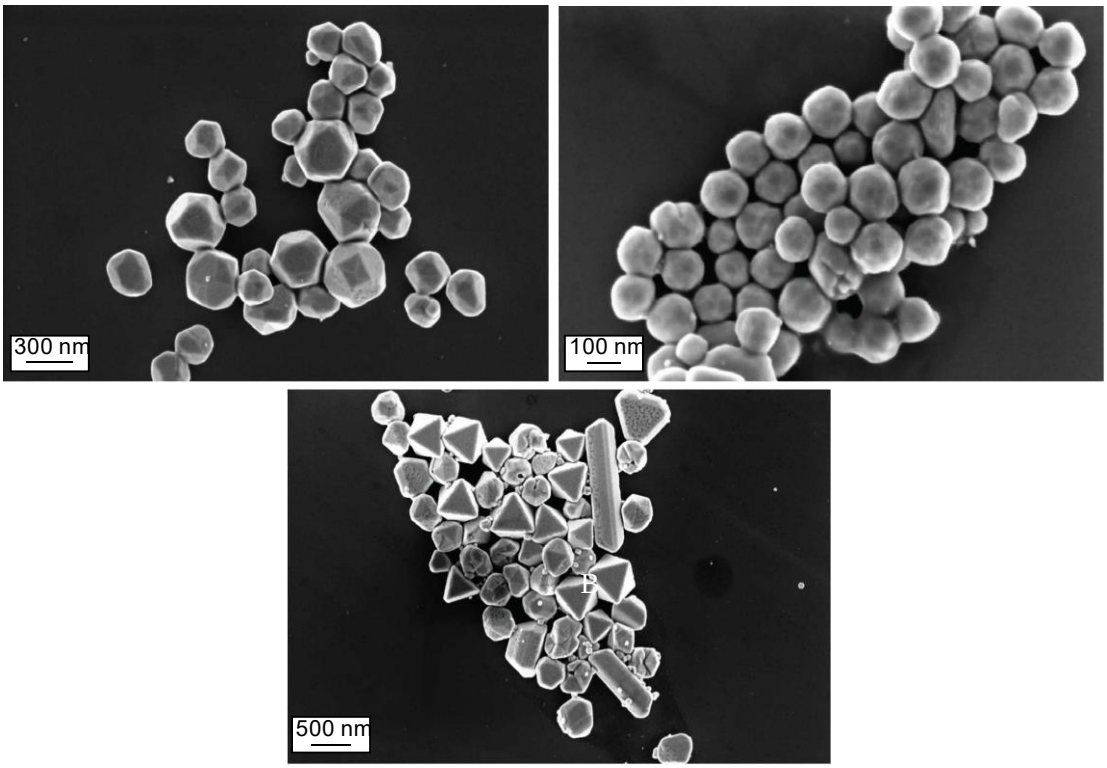

Figure 3.2: SEM images of failed attempts to synthesize Ag OHN. **(A)** Ag OHN synthesis beginning with old Ag NC led to irregular Ag NP after 30 min. **(B)** Ag OHN synthesis started with old NC and double the standard volume of 3.44 mM Cu^{2+} resulted in rounded, irregular Ag NP. **(C)** Ag OHN Synthesis beginning with fresh NC and twice the standard volume of 3.44 mM Cu^{2+} produced a mixture of Ag OHN, rods, triangular NP, and other irregular NP. All three reactions took place at 185-190°C with 180 mM PVP.

extended periods of time began to lose the sharpness of their sides and possibly degraded as well. No fully successful Ag OHN synthesis resulted from old NC. Similarly, no Ag OHN were ever synthesized using 25 µL 3.44 mM Cu^{2+} (0.086 µmoles Cu^{2+}) in place of the 50 µL (0.172 µmoles Cu^{2+}) originally used in the synthesis. However, it was found that both 50 µL (0.172 µmoles Cu^{2+}) and 100 µL of 3.44 mM Cu^{2+} (0.344 µmoles Cu^{2+}) did result in OHN formation. The flasks originally being used for the synthesis were replaced, assuming the scratches in the glassware were giving the $AgNO_3$ a nucleation point to form irregular NP. In an attempt to slow down the OHN formation to prevent the irregular NP formation, a flow rate of 400 µL·min^{-1} was employed, which was found to be successful to form Ag OHN under one set of reaction conditions. The last alteration was an increased heat for the reaction. When the temperature of the reaction was increased from 190°C to 194-196°C, OHN were observed under conditions previously determined to not form OHN. A summary of OHN syntheses conditions and outcomes just discussed are presented in **Table 3.1.**

The conditions of synthesis that were successful and therefore considered to be the standard synthesis moving forward to the Ag^+ measurements were using freshly synthesized NC with 50 µL 3.44 mM Cu^{2+} (0.172 µmol Cu^{2+}) in the unscratched flasks. The 235 mM $AgNO_3$ and 180 mM PVP were delivered with a flow rate of 500 µL·min^{-1} after the temperature of the oil bath was between 193-196°C. SEM images of a successful Ag OHN synthesis at several time points are visible in **Figure 3.3**. It can be noticed in the last two time points small, round Ag NP are present. These small NP commonly formed if the OHN synthesis continued to have $AgNO_3$ injected into the system after the OHN had fully formed. This is likely due to the OHN growth becoming less kinetically favorable after a specific OHN size is reached than formation of small, round Ag NP.

Despite being able to sample a single OHN synthesis at several times for SEM, each time point for the Ag ISE measurements represents an individual OHN synthesis due to the likelihood that removing a large sample would alter the system and disrupt the OHN formation. In **Figure 3.4**, the measured concentration is shown versus time of the reaction in min. The Ag^+ concentration for the first three time points are similar,

Table 3.1: Ag OHN synthesis conditions altered and the outcome of the synthesis. All reactions utilized 235 mM $AgNO_3$ and 180 mM PVP (based on monomer). For reactions that formed OHN, the Ag OHN were visible under SEM between 20 and 30 min regardless of flow rate.

Fresh or Old NC used	Micromoles Cu^{2+} Added (µmole)	Flask utilized	Flow Rate ($\mu L \cdot min^{-1}$)	Average Reaction Temperature (°C)	Ag NP formed
Old	0.344	Scratched	500	190	Irregular
Old	0.172	Scratched	500	190	Irregular
Fresh	0.344	Scratched	500	190	Mix
Fresh	0.344	Scratched	400	190	Irregular
Fresh	0.172	Scratched	500	194	Irregular
Fresh	0.344	Unscratched	400	195	OHN
Fresh	0.172	Unscratched	500	190	Irregular
Fresh	0.172	Unscratched	500	195	OHN
Fresh	0.086	Unscratched	500	195	Irregular

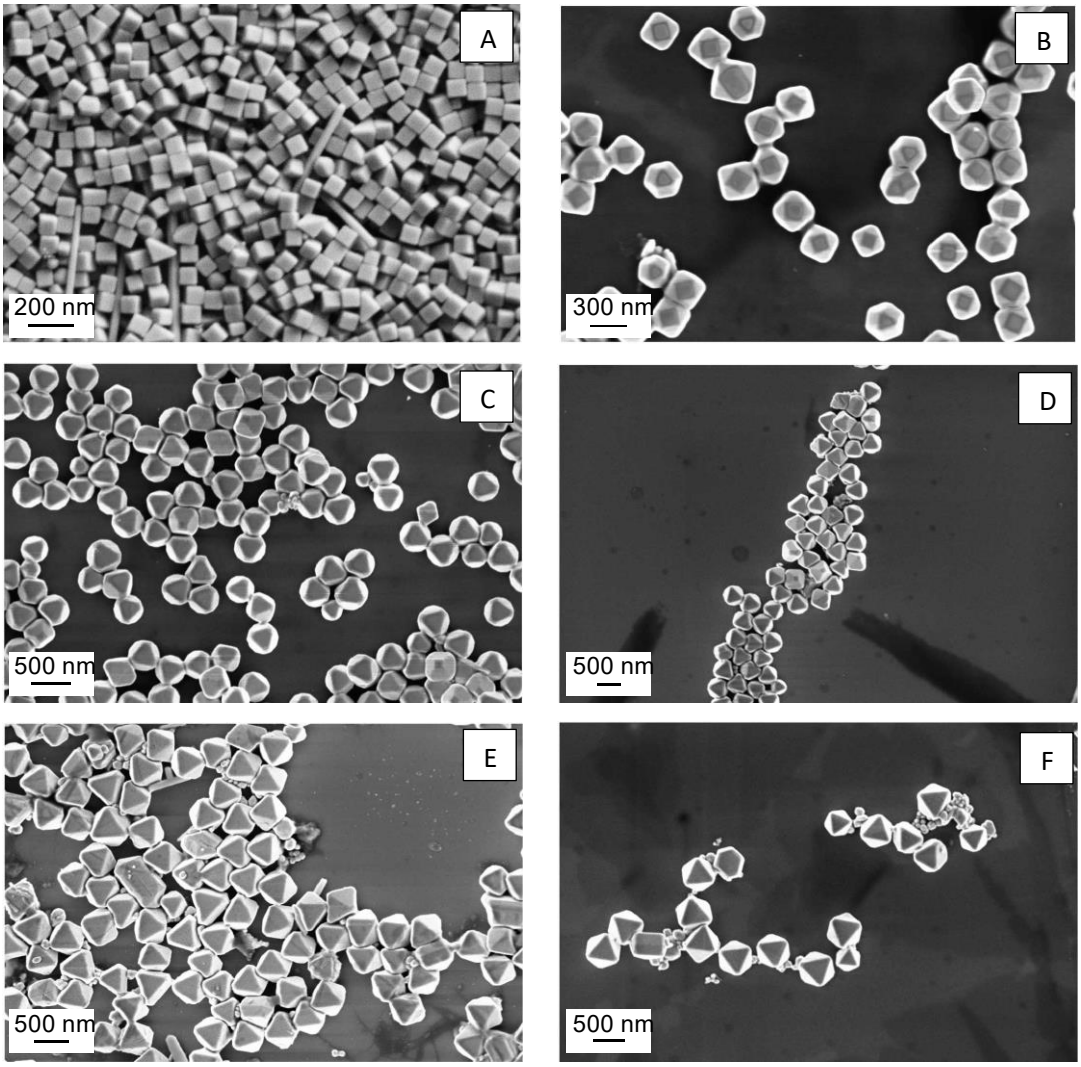

Figure 3.3: SEM images of a successful Ag OHN synthesis from Ag NC seeds at various time points under the established standard reaction conditions. **(A)** 0 min, **(B)** 5 min, **(C)** 10 min, **(D)** 15 min, **(E)** 20 min, **(F)** 25 min.

indicating Ag^+ consumption, while the measured Ag^+ at 30 min is significantly different. For a typical OHN synthesis, approximately 30 min is when the OHN have fully formed and the small, round Ag NP begin to form. Based on SEM images, the OHN were not fully formed for the synthesis measured at 30 min, but there were the beginnings of the small NP formation. This Ag^+ concentration could potentially increase at this time point due to the end of the OHN formation, where a buildup of $AgNO_3$ in the system leads to the formation of the round NP. However, it is also a possibility that the concentration measured is due to an unsuccessful synthesis of OHN. Based on the SEM images, it is more likely because the OHN formation was not complete at 30 min, which could indicate either the synthesis needed to be allowed to react longer or the synthesis would produce just irregular NP, not OHN. In order to determine the true concentration of Ag^+, the 30 min time point would need to be repeated, multiple times.

Through this work, the synthesis of Ag OHN was potentially optimized, leading to consistent formation of Ag OHN. It remains unclear as to why the synthesis conditions that previously produced the Ag OHN was no longer a viable method to synthesize Ag OHN. From the Ag ISE data, unfortunately, no conclusions can be made about the kinetics of the reaction. It is possible Ag ISE is not the most useful method to study Ag OHN formation. An *in-situ* monitoring process may be optimal for this system. Regardless, it is possible the Ag^+ measurements may provide useful data and mechanistic information about the formation of the secondary, round Ag NP, as well.

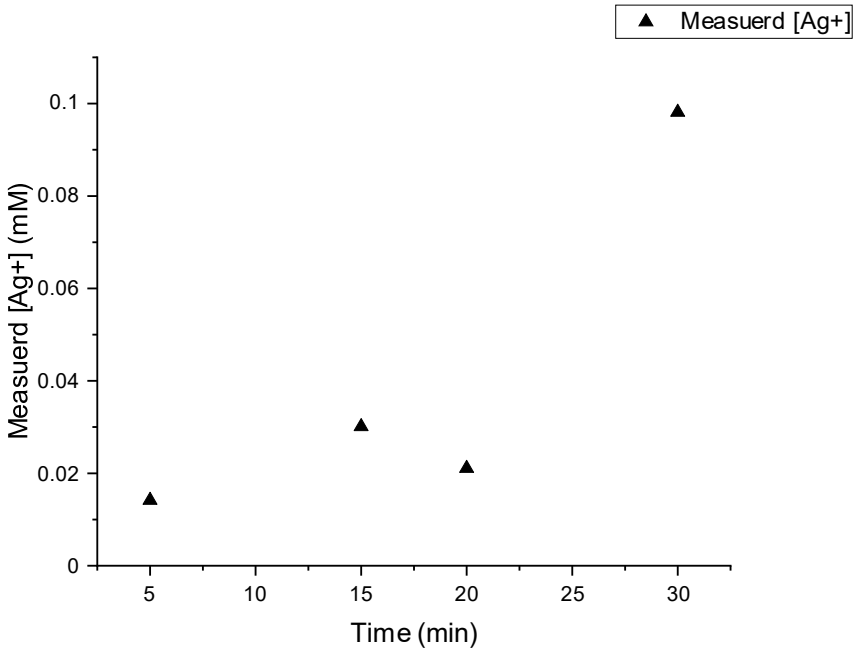

Figure 3.4: Ag ISE measurements of Ag^{+} concentration as a function of time for multiple Ag OHN syntheses at 195°C with 235 mM $AgNO_3$ and 180 mM PVP at the time points 5, 15, 20, and 30 min.

CHAPTER 4. FUTURE WORK AND DIRECTIONS

Future of Silver Nanocube Synthesis

Through the work presented on Ag NC synthesis, it was noted that there is likely a constant number of Ag seeds that form into approximately the same number of Ag NC despite the initial concentration of Ag^+, due to the size differences in the NC at different concentrations of Ag^+. The rate of the NC growth depended on the PVP:Ag ratio due to dilution of Ag^+ leading to lower probability of molecular interactions between Ag atoms and Ag atoms with PVP. I concluded the Finke-Watzky mechanism was apparent for multiple PVP:Ag ratios. However, more work focused on studying the concentration of Ag^+ over time for various reaction conditions are needed. The work presented for 55 mM Ag is not finished, and this would be a great place for the work to be continued. Ideally, to prove the synthesis mechanism proceeds through an autocatalytic step, several more concentrations of Ag should be investigated. A recommendation of the concentrations to investigate would be from 55 mM Ag through 150 mM Ag. The outcome of that work would highlight several higher and lower PVP:Ag ratios. If all of the Ag ISE data gathered demonstrated a two-step mechanism, it would show that the synthesis always operates via a slow reduction by the PVP, followed by fast autocatalysis.

A second direction for this project is to use small angle X-ray scattering (SAXS) to determine concentrations of the Ag NC after synthesis. Previous work in the group has measured concentrations of metal ions with ICP-OES. The concentration of Ag^+ present in a NC sample can be measured; however, this does not provide the concentration of NC present, which SAXS can. Preliminary SAXS measurements have been made, in addition to some troubleshooting efforts while taking the measurements. **Figure 4.1**, shows some of the SAXS measurements made along with modeling of the expected spectra for the NC based on their radius (half of the average length of the NC sample). To continue this work, more modeling would need to be completed to solve for the scattering contrast for our materials. The size of the Ag NC would also have to be determined more accurately as the size was estimated based on individual measurements of approximately 100-150 Ag NC per sample. Our group has recently

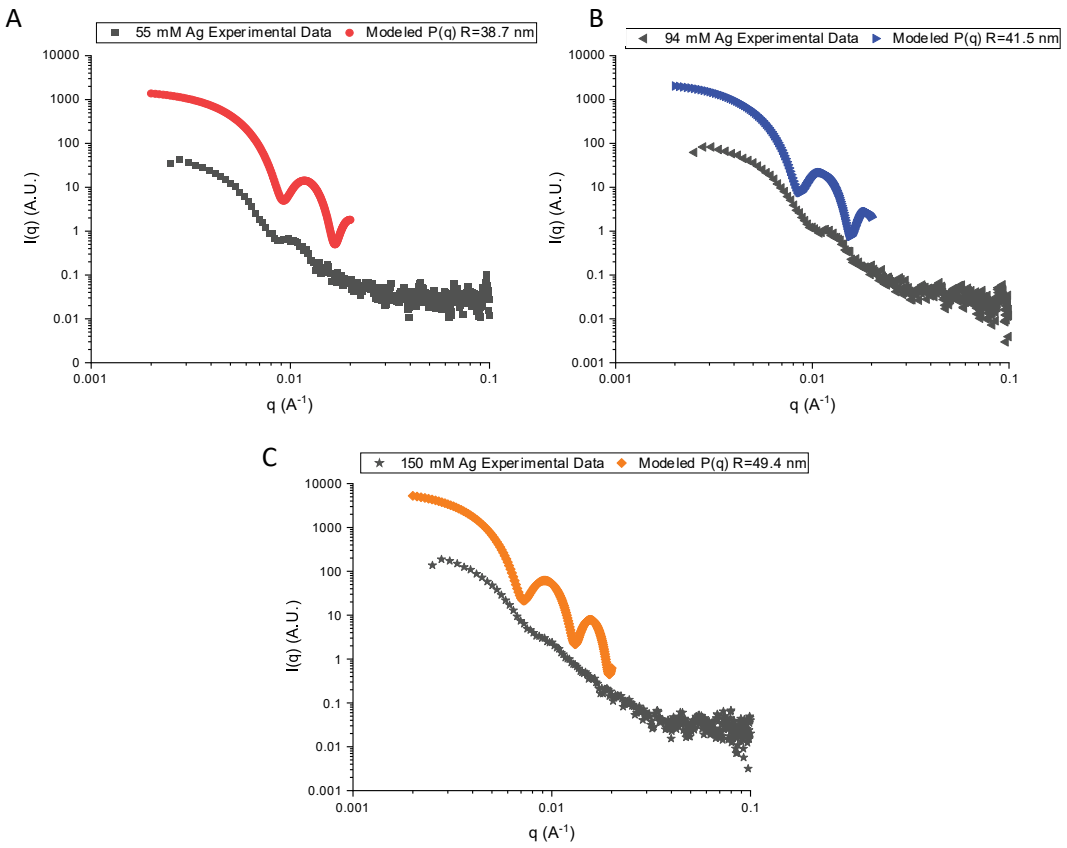

Figure 4.1: SAXS data for three differently sized Ag NC synthesized. All measured data is the result of 5 µL aliquot of Ag NC in EG (uncleaned) being further diluted by EG in 1.0 mm quartz capillaries. Radii were obtained by measuring the diameter via SEM images of the specific NC sample and dividing by 2. **(A)** Ag NC synthesized with 55 mM Ag^+ with an average radius of 38.7 nm. The measured data is shown as black squares, while the modeled data is displayed as red circles**. (B)** Ag NC formed from 94 mM Ag^+ (standard synthesis) with an average radius of 41.5 nm. Black, left-pointing triangles denote experimental data, while the blue, right-pointing triangles denote modeled data**. (C)** Ag NC synthesized from 150 mM Ag^+ with an average radius of 49.4 nm. Black stars represent measured data, while the orange diamonds display the modeled data.

improved a Matlab program written to size our Ag NC, that will automatically measure all NC in an SEM image and remove measurements that are considered a statistic outlier. With this program, thousands of NC would be measured, leading to much more accurate averages of NC diameter and it would give a better idea of the dispersity within the sample. If the SAXS measurements can be shown to accurately measure the Ag NC concentration for our system, the samples can be quantified in another way, which could also help to understand how changing reaction conditions affects yield in addition to giving mechanistic insight.

A final possible direction is a study to determine success of the synthesis and quantify the variation between samples. For the current method to form Ag NC, it is unknown how frequently the reactions fail, or what causes the reactions to fail, as the failed reactions have never been characterized. In addition to the unknown failure rate, the variation from one synthesis to another is quite evident in **Figure 2.4** due to large error bars at certain time points. There were several attempts to mitigate the variation between syntheses by changing conditions such as air flow, reaction placement, oil baths, etc., but all attempts were unsuccessful and sometimes detrimental to the Ag NC fromation. Determining the cause of the variation or developing a statistical program to rule individual syntheses as outliers would be incredibly helpful for analysis of the synthesis, especially for future Ag ISE measurements.

Future of Silver Octahedron Synthesis

The outcome of the investigation of Ag OHN formation was that the synthesis was enhanced to lead to consistent Ag OHN formation, which was not the result of the previously established method. After the synthesis was found to produce OHN, the kinetics of the reaction began to be examined, but no conclusions could yet be drawn. The next steps of this work would be to repeat all of the Ag^+ measurements made at 5, 15, 20, and 30 min multiple times, to ensure the data accurately reflects an average Ag OHN synthesis. Additional time points such as 10, 25, 35, 40, and 45 min should also be conducted. From this, the mechanism of formation may be revealed, similar to how the Finke-Watzky model was evident for the Ag NC. Once the Ag^+ concentration as a function of time is determined for the standard OHN synthesis, the kinetics of altered

syntheses could also be investigated. As previously mentioned, when metals with higher SRP than Ag, such as Pd and Au, are used to synthesize Ag OHN, it is thought that the foreign metal deposits via GRR. Measurements of Ag OHN synthesis utilizing Au^{3+} or Pd^{2+} will likely result in vastly different concentrations of Ag^{+} as time progresses in the synthesis.

References:

1. Jeevanandam, J.; Barhoum, A.; Chan, Y. S.; Dufresne, A.; Danquah, M. K., Review on nanoparticles and nanostructured materials: history, sources, toxicity and regulations. *Beilstein J. Nanotechnol.* **2018,** *9*, 1050-1074.
2. Kovalenko, M. V.; Manna, L.; Cabot, A.; Hens, Z.; Talapin, D. V.; Kagan, C. R.; Klimov, V. I.; Rogach, A. L.; Reiss, P.; Milliron, D. J.; Guyot-Sionnnest, P.; Konstantatos, G.; Parak, W. J.; Hyeon, T.; Korgel, B. A.; Murray, C. B.; Heiss, W., Prospects of Nanoscience with Nanocrystals. *ACS Nano* **2015,** *9* (2), 1012-1057.
3. Nozik, A. J., Photoelectrochemistry: Applications to Solar Energy Conversion. *Ann. Rev. Phys. Chem.* **1978,** *29*, 189-222.
4. Rossetti, R.; Nakahara, S.; Brus, L. E., Quantum size effects in the redox potentials, resonance Raman spectra, and electronic spectra of CdS crystallites in aqueous solution. *J. Chem. Phys* **1983,** *79* (2), 1086-1088.
5. Somorjai, G. A., Modern Surface Science and Surface Technologies: An Introduction. *Chem. Rev.* **1996,** *96* (4), 1223-1236.
6. C.B.Murray; D.J.Norris; Bawendi, M. G., Synthesis and characterization of nearly monodisperse CdE (E = sulfur, selenium, tellurium) semiconductor nanocrystallites. *J. Am. Chem. Soc.* **1993,** *115* (19), 8706-8715.
7. An, K.; Somorjai, G. A., Size and Shape Control of Metal Nanoparticles for Reaction Selectivity in Catalysis. *ChemCatChem.* **2012,** *4*, 1512-1524.
8. Ruditskiy, A.; H.-C.Peng; Xia, Y., Shape-Controlled Metal Nanocrystals for Heterogeneous Catalysis. *Annu. Rev. Chem. Biomol. Eng.* **2016,** *7*, 327-348.
9. Lewis, L. N., Chemical catalysis by colloids and clusters. *Chem. Rev.* **1993,** *93*, 2693-2730.
10. Liu, J., Catalysis by Supported Single Metal Atoms. *ACS Catal.* **2017,** *7*, 34-59.
11. Roduner, E., Size matters: why nanomaterials are different. *Chem. Soc. Rev.* **2006,** *35*, 583-592.
12. Taylor, S.; Lemire, G. W.; Hamrick, Y. M.; Fu, Z.; Morse, M. D., Resonant two-photon ionization spectroscopy of jet-cooled Pt_2. *J. Chem. Phys* **1988,** *89*, 5517-5523.
13. Johnston, R. L., *Metal Nanoparticles and Nanoalloys*. Elsevier, 2012; Vol. 3, p 1-42.
14. Shang, L.; Xu, J.; Nienhaus, G. U., Recent advances in synthesizing metal nanocluster-based nanocomposites for application in sensing, imaging and catalysis. *Nano Today* **2019,** *28*, 100767.
15. Eychmu1ller, A., Structure and Photophysics of Semiconductor Nanocrystals. *J. Phys. Chem. B* **2000,** *104*, 6514-6528.
16. Desireddy, A.; Conn, B. E.; Guo, J.; Yoon, B.; Barnett, R. N.; Monahan, B. M.; Kirschbaum, K.; Griffith, W. P.; Whetten, R. L.; Landman, U.; Bigioni, T. P., Ultrastable silver nanoparticles. *Nature* **2013,** *501* (7467), 399-402.
17. Zhang, Q.; Moran, C. H.; Xia, X.; Rycenga, M.; Li, N.; Xia, Y., Synthesis of Ag Nanobars in the Presence of Single-Crystal Seeds and a Bromide Compound, and Their Surface-Enhanced Raman Scattering (SERS) Properties. *Langmuir* **2012,** *28* (24), 9047-9054.
18. Tao, A.; Sinsermsuksakul, P.; Yang, P., Polyhedral Silver Nanocrystals with Distinct Scattering Signatures. *Angew. Chem. Int. Ed.* **2006,** *45*, 4597-4601.

19. Wiley, B. J.; Chen, Y.; McLellan, J. M.; Xiong, Y.; Li, Z.-Y.; Ginger, D.; Xia, Y., Synthesis and Optical Properties of Silver Nanobars and Nanorice. **2007,** *7* (4), 1032-1036.
20. Nie, S.; Emory, S. R., Probing Single Molecules and Single Nanoparticles by Surface-Enhanced Raman Scattering. *Science* **1997,** *275* (5303), 1102-1106.
21. Yaraki, M. T.; Rezaei, S. D.; Tan, Y. N., Simulation guided design of silver nanostructures for plasmon-enhanced fluorescence, singlet oxygen generation and SERS applications. *Phys. Chem. Chem. Phys.* **2020,** *22* (5673-5687).
22. Christopher, P.; Linic, S., Shape- and Size-Specific Chemistry of Ag Nanostructures in Catalytic Ethylene Epoxidation. *ChemCatChem* **2010,** *2*, 78-83.
23. Ruditskiy, A.; Peng, H.-C.; Xia, Y., Shape-Controlled Metal Nanocrystals for Heterogeneous Catalysis. *Annu. Rev. Chem. Biomol. Eng.* **2016,** *7*, 327-348.
24. Stamenkovic, V. R.; Fowler, B.; Mun, B. S.; Wang, G.; Ross, P. N.; Lucas, C. A.; Marković, N. M., Improved Oxygen Reduction Activity on Pt3Ni(111) via Increased Surface Site Availability. *Science* **2007,** *315* (5811), 493-497.
25. Christopher, P.; Linic, S., Engineering Selectivity in Heterogeneous Catalysis: Ag Nanowires as Selective Ethylene Epoxidation Catalysts. *J. Am. Chem. Soc.* **2008,** *130* (34), 11264-11265.
26. Peng, H.-C.; Xie, S.; Park, J.; Xia, X.; Xia, Y., Quantitative Analysis of the Coverage Density of Br– Ions on Pd{100} Facets and Its Role in Controlling the Shape of Pd Nanocrystals. *J. Am. Chem. Soc.* **2013,** *135* (10), 3780-3783.
27. Fiévet, F.; Ammar-Merah, A.; Brayner, R.; Chau, F.; Giraud, M.; Mammeri, F.; Peron, J.; Piquemal, J.-Y.; Sicard, L.; Viau, G., The polyol process: a unique method for easy access to metal nanoparticles with tailored sizes, shapes and compositions. *Chem. Soc. Rev.* **2018,** *47*, 5187-5233.
28. Qi, X.; Fichthorn, K. A., Theory of the thermodynamic influence of solution-phase additives in shape-controlled nanocrystal synthesis. *Nanoscale* **2017,** *9*, 15635-15642.
29. Biacchi, A. J.; Schaak, R. E., The Solvent Matters: Kinetic versus Thermodynamic Shape Control in the Polyol Synthesis of Rhodium Nanoparticles. *ACS Nano* **2011,** *5* (10), 8089-8099.
30. Grzelczak, M.; Pérez-Juste, J.; Mulvaney, P.; Liz-Marzán, L. M., Shape control in gold nanoparticle synthesis. *Chem. Soc. Rev.* **2008,** *37*, 1783-1791.
31. Wiley, B.; Sun, Y.; Mayers, B.; Xia, Y., Shape-Controlled Synthesis of Metal Nanostructures: The Case of Silver. *Chem. Eur. J.* **2004,** *11*, 454-463.
32. Hughes, B. K.; Luther, J. M.; Beard, M. C., The Subtle Chemistry of Colloidal, Quantum-Confined Semiconductor Nanostructures. *ACS Nano* **2012,** *6* (6), 4573-4579.
33. Tang, Z.; Zhang, Q.; Yin, Y.; Chang, C. A., Facet Selectivity of Ligands on Silver Nanoplates: Molecular Mechanics Study. *J. Phys. Chem. C* **2014,** *118* (37), 21589-21598.
34. Qi, X.; Balankura, T.; Zhou, Y.; Fichthorn, K. A., How Structure-Directing Agents Control Nanocrystal Shape: Polyvinylpyrrolidone-Mediated Growth of Ag Nanocubes. *Nano Lett.* **2015,** *15* (11), 7711-7717.
35. Chen, Z.; Chang, J. W.; Balasanthiran, C.; Milner, S. T.; Rioux, R. M., Anisotropic Growth of Silver Nanoparticles Is Kinetically Controlled by Polyvinylpyrrolidone Binding. *J. Am. Chem. Soc.* **2019,** *141* (10), 4328-4337.

36. Jharimune, S.; Pfukwa, R.; Chen, Z.; Anderson, J.; Klumperman, B.; Rioux, R. M., Chemical Identity of Poly(N-vinylpyrrolidone) End Groups Impact Shape Evolution During the Synthesis of Ag Nanostructures. *J. Am. Chem. Soc.* **2021,** *143* (1), 184-195.
37. Jin, M.; Liu, H.; Zhang, H.; Xie, Z.; Liu, J.; Xia, Y., ynthesis of Pd Nanocrystals Enclosed by {100} Facets and with Sizes <10 nm for Application in CO Oxidation. *Nano Res.* **2011,** *4* (1), 83-91.
38. Borodko, Y.; Habas, S. E.; Koebel, M.; Yang, P.; Frei, H.; Somorjai, G. A., Probing the Interaction of Poly(vinylpyrrolidone) with Platinum Nanocrystals by UV−Raman and FTIR. *J. Phys. Chem. B* **2006,** *110* (46), 23052-23059.
39. Sadakiyo, M.; Kon-no, M.; Sato, K.; Nagaoka, K.; Kasai, H.; Kato, K.; Yamauch, M., Synthesis and catalytic application of PVP-coated Ru nanoparticles embedded in a porous metal–organic framework. *Dalton Trans.* **2014,** *43*, 11295-11298.
40. Wang, Y.; Wan, D.; Xie, S.; Xia, X.; Huang, C. Z.; Xia, Y., Synthesis of Silver Octahedra with Controlled Sizes and Optical Properties via Seed-Mediated Growth. *ACS Nano* **2013,** *7* (5), 4586-4594.
41. Pastoriza-Santos, I.; Liz-Marzán, L. M., Synthesis of Silver Nanoprisms in DMF. *Nano Lett.* **2002,** *2* (8), 903-905.
42. Chen, Z.; T.Balankura; Fichthorn, K. A.; Rioux, R. M., Revisiting the Polyol Synthesis of Silver Nanostructures: Role of Chloride in Nanocube Formation. *ACS Nano* **2019,** *13* (2), 1849-1860.
43. Djafari, J.; Fernández-Lodeiro, A.; García-Lojo, D.; Fernández-Lodeiro, J.; Rodríguez-González, B.; Pastoriza-Santos, I.; Pérez-Juste, J.; Capelo, J. L.; Lodeiro, C., Iron(II) as a Green Reducing Agent in Gold Nanoparticle Synthesis. *ACS sustainable Chem. Eng.* **2019,** *7* (9), 8295-8302.
44. Kim, M. J.; Alvarez, S.; Chen, Z.; Fichthorn, K. A.; Wiley, B. J., Single-Crystal Electrochemistry Reveals Why Metal Nanowires Grow. *J. Am. Chem. Soc.* **2018,** *140* (44), 14740-14746.
45. Tsuji, M.; Gomi, S.; Maeda, Y.; Matsunaga, M.; Hikino, S.; Uto, K.; Tsuji, T.; Kawazumi, H., Rapid Transformation from Spherical Nanoparticles, Nanorods, Cubes, or Bipyramids to Triangular Prisms of Silver with PVP, Citrate, and H_2O_2. *Langmuir* **2012,** *28* (24), 8845-8861.
46. Wiley, B. J.; Xiong, Y.; Li, Z.-Y.; Yin, Y.; Xia, Y., Right Bipyramids of Silver: A New Shape Derived from Single Twinned Seeds. *Nano Lett.* **2006,** *6* (4), 765-768.
47. Im, S. H.; Lee, Y. T.; Wiley, B.; Xia, Y., Large-Scale Synthesis of Silver Nanocubes: The Role of HCl in Promoting Cube Perfection and Monodispersity. *Angew. Chem. Int. Ed.* **2005,** *44*, 2154-2157.
48. Sun, Y.; Xia, Y., Shape-Controlled Synthesis of Gold and Silver Nanoparticles. *Science* **2002,** *298* (5601), 2176-2179.
49. Skrabalak, S. E.; Wiley, B. J.; Kim, M.; Formo, E. V.; Xia, Y., On the Polyol Synthesis of Silver Nanostructures: Glycolaldehyde as a Reducing Agent. *Nano Lett.* **2008,** *8* (7), 2077-2081.
50. Xia, X.; Zeng, J.; Oetjen, L. K.; Li, Q.; Xia, Y., Quantitative Analysis of the Role Played by Poly(vinylpyrrolidone) in Seed-Mediated Growth of Ag Nanocrystals. *J. Am. Chem. Soc.* **2012,** *134* (3), 1793-1801.

51. Wang, Y.; Zheng, Y.; Huang, C. Z.; Xia, Y., Synthesis of Ag Nanocubes 18–32 nm in Edge Length: The Effects of Polyol on Reduction Kinetics, Size Control, and Reproducibility. *J. Am. Chem. Soc.* **2013,** *135* (5), 1941-1951.
52. Y. Sun; Mayers, B.; Herricks, T.; Xia, Y., Polyol Synthesis of Uniform Silver Nanowires: A Plausible Growth Mechanism and the Supporting Evidence. *Nano Lett.* **2003,** *3* (7), 955-960.
53. Al-Saidi, W. A.; Feng, H.; Pichthorn, K. A., Adsorption of Polyvinylpyrrolidone on Ag Surfaces: Insight into a Structure-Directing Agent. *Nano Lett.* **2012,** *12*, 997-1001.
54. Smith, J. G.; Yang, Q.; Jain, P. K., Identification of a Critical Intermediate in Galvanic Exchange Reactions by Single-Nanoparticle-Resolved Kinetics. *Angew. Chem.* **2014,** *126*, 2911-2916.
55. Zhang, W.; Yang, J.; Lu, X., Tailoring Galvanic Replacement Reaction for the Preparation of Pt/Ag Bimetallic Hollow Nanostructures with Controlled Number of Voids. *ACS Nano* **2012,** *6* (8), 7397-7405.
56. Zhang, W.; Tan, F.; Wang, W.; Qiu, X.; Qiao, X.; Chen, J., Facile, template-free synthesis of silver nanodendrites with high catalytic activity for the reduction of p-nitrophenol. *J. Hazard. Mater.* **2012,** *217-218*, 36-42.
57. Personick, M. L.; Langille, M. R.; Zhang, J.; Mirkin, C. A., Shape Control of Gold Nanoparticles by Silver Underpotential Deposition. *Nano Lett.* **2011,** *11* (8), 3394-3398.
58. Ma, L.; Wang, C.; Xia, B. Y.; Mao, K.; He, J.; Wu, X.; Xiong, Y.; Lou, X. W., Platinum Multicubes Prepared by Ni^{2+}-Mediated Shape Evolution Exhibit High Electrocatalytic Activity for Oxygen Reduction. *Angew. Chem. Int. Ed.* **2015,** *54*, 5666-5671.
59. Wiley, B.; Sun, Y.; Xia, Y., Polyol Synthesis of Silver Nanostructures: Control of Product Morphology with Fe(II) or Fe(III) Species. *Langmuir* **2005,** *21* (18), 8077-8080.
60. Bastús, N. G.; Merkoçi, F.; Piella, J.; Puntes, V., Synthesis of Highly Monodisperse Citrate-Stabilized Silver Nanoparticles of up to 200 nm: Kinetic Control and Catalytic Properties. *Chem. Mater.* **2014,** *26* (9), 2836-2846.
61. Xiong, Y.; Washio, I.; Chen, J.; Cai, H.; Li, Z.-Y.; Xia, Y., Poly(vinyl pyrrolidone): A Dual Functional Reductant and Stabilizer for the Facile Synthesis of Noble Metal Nanoplates in Aqueous Solutions. *Langmuir* **2006,** *22* (20), 8563-8570.
62. Li, S. F.; Zhang, H. Y., Effect of Polyvinylpyrrolidone on the Preparation of Silver Nanowires. *Adv. Mat. Res.* **2014,** *881-883*, 940-943.
63. Watzky, M. A.; Finke, R. G., Transition Metal Nanocluster Formation Kinetic and Mechanistic Studies. A New Mechanism When Hydrogen Is the Reductant: Slow, Continuous Nucleation and Fast Autocatalytic Surface Growth. *J. Am. Chem. Soc.* **1997,** *119* (43), 10382-10400.
64. Tao, A.; Sinsermsuksakul, P.; Yang, P., Polyhedral Silver Nanocrystals with Distinct Scattering Signatures. *Angew. Chem. Int. Ed.* **2006,** *45*, 4597-4601.